



Extremely efficient electrochemical degradation of organic pollutants with co-generation of hydroxyl and sulfate radicals on Blue-TiO₂ nanotubes anode



Jingju Cai^{a,b,c,d}, Minghua Zhou^{a,b,c,d,*}, Yuwei Pan^{a,b,c,d}, Xuedong Du^{a,b,c,d}, Xiaoye Lu^{a,b,c,d}

^a Key Laboratory of Pollution Process and Environmental Criteria, Ministry of Education, College of Environmental Science and Engineering, Nankai University, Tianjin 300350, China

^b Tianjin Key Laboratory of Environmental Technology for Complex Trans-Media Pollution, Nankai University, Tianjin 300350, China

^c Tianjin Key Laboratory of Urban Ecology Environmental Remediation and Pollution Control, College of Environmental Science and Engineering, Nankai University, Tianjin 300350, China

^d Tianjin Advanced Water Treatment Technology International Joint Research Center, College of Environmental Science and Engineering, Nankai University, Tianjin 300350, China

ARTICLE INFO

Keywords:

TiO₂nanotubes
Electrochemical advanced oxidation processes
Boron-doped diamond
Phenol degradation
Hydroxyl radical and sulfate radical

ABSTRACT

Efficient anode materials are essential to electrochemical advanced oxidation processes (EAOPs) for organic wastewater treatment. In this regard, blue TiO₂ nanotube arrays (Blue-TNA) anode was prepared for the first time in formic acid electrolyte by electrochemical self-doping and applied for electrochemical degradation of contaminants. Characterized by XPS, Raman and Mott-Schottky curves, the formation of Ti³⁺ on Blue-TNA was confirmed. This anode was more efficient and had a higher hydroxyl radical production activity (1.7×10^{-14} M) than BDD (9.8×10^{-15} M), inducing a higher TOC and COD removal of 100 mg/L phenol with a lower energy consumption of 9.9 kW h/(kg COD) at current density 2.5 mA/cm², pH 5 in 0.1 M Na₂SO₄, account for the lower accumulation of degradation intermediates. Both 'OH and SO₄²⁻ were responsible for the degradation on Blue-TNA anode, while their contributions differed greatly with that of BDD, and could be affected and regulated by the operating parameters like current density, initial pH and Na₂SO₄ concentration. Blue-TNA anode represented a relative stable performance for 5 cycles degradation of 100 mg/L phenol for each cycle of 300 min, and such an oxidation capacity could be easily regenerated by electrochemical reduction in formic acid. Blue-TNA anode had an excellent performance on the TOC removal and MCE especially at low current density of 2.5 mA/cm² when compared with other anodes. Therefore, Blue-TNA anode is hopeful a promising and cost-effective anode for electrochemical oxidation.

1. Introduction

Based on the electrochemical generation of powerful oxidants such as hydroxyl radical ('OH), electrochemical advanced oxidation processes (EAOPs) have been successfully developed to destroy various organic pollutants up to their mineralization for wastewater treatment in the past two decades [1–3]. Previous studies have confirmed the essential influence of the anode material nature on both treatment efficiency and selectivity [4,5]. Generally, there are two types of anode materials: (1) active anodes (Pt, IrO₂ and RuO₂) with low O₂ over-potential and (2) non-active anodes (SnO₂, PbO₂ and boron-doped diamond (BDD)) with high O₂ over-potential [6]. It is supposed that the

anode M reacts with H₂O to produce the physisorbed hydroxyl radical (M('OH)) through eq.(1), rendering the degradation or mineralization of organic pollutants [6]. The surface of active anode interacts strongly with 'OH to form higher oxide or superoxide (MO) through eq.(2). However, the surface of a non-active anode interacts so weakly with 'OH that allows the direct reaction of organic pollutants (R) with M ('OH) to give fully oxidized reaction (3) [7].



* Corresponding author at: Key Laboratory of Pollution Process and Environmental Criteria, Ministry of Education, College of Environmental Science and Engineering, Nankai University, Tianjin 300350, China.

E-mail address: zhoumh@nankai.edu.cn (M. Zhou).

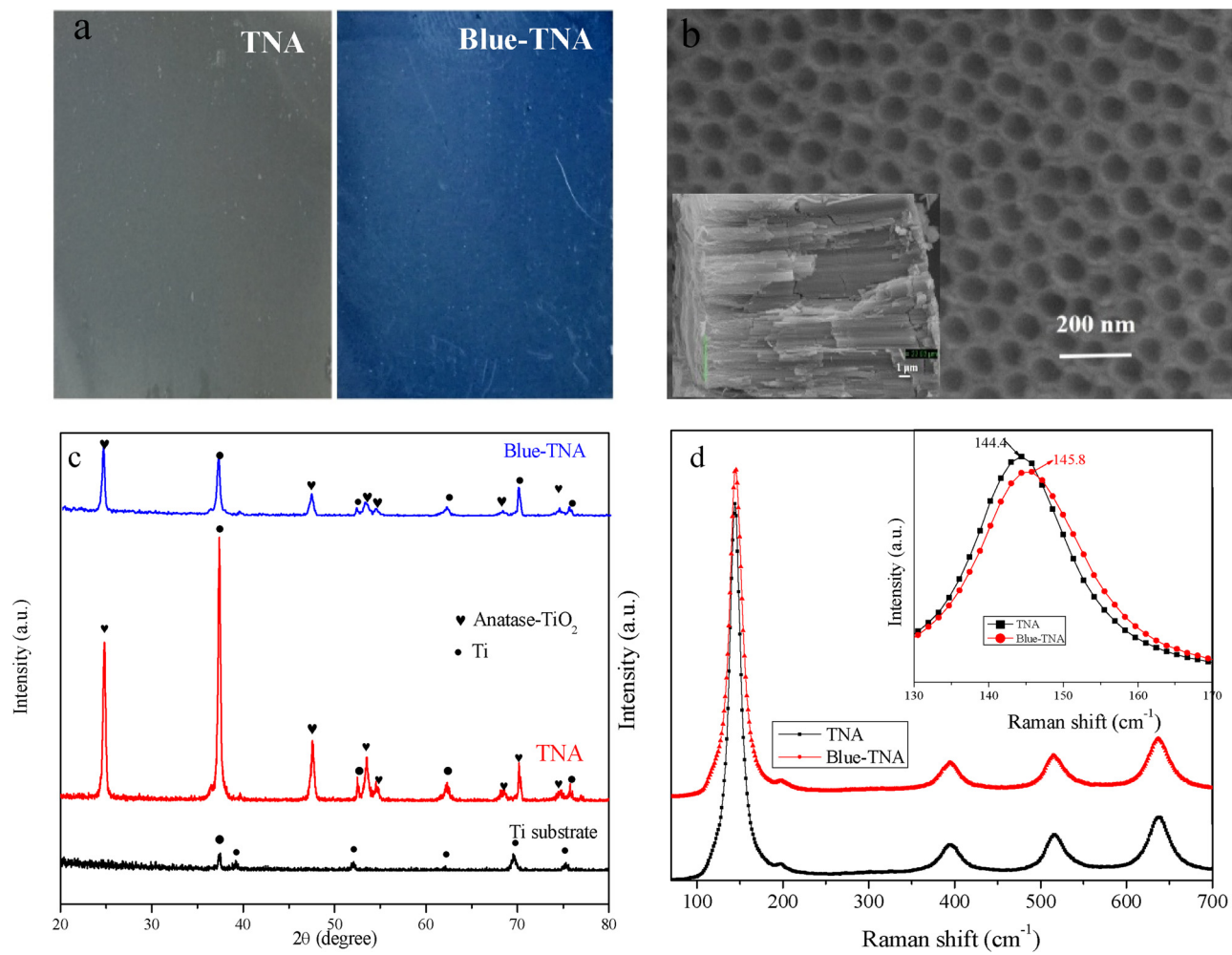


Fig. 1. SEM images of (a) the color of TNA and Blue-TNA (b) TNA (c) XRD patterns of TNA and Blue-TNA (d) Raman spectra of TNA and Blue-TNA. The inset shows the corresponding main Eg Raman mode of samples.

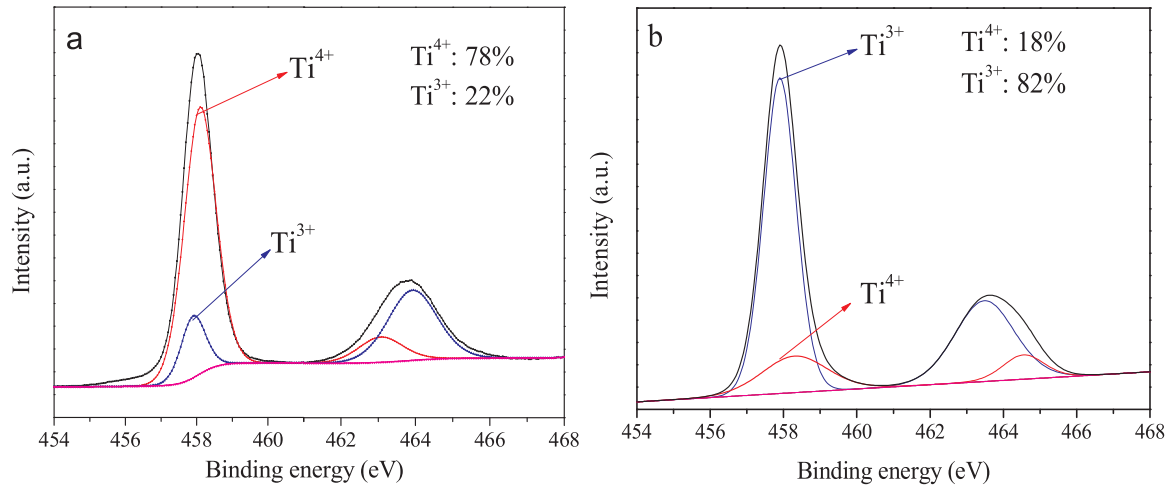


Fig. 2. XPS spectra of (a) TNA (b) Blue-TNA.

Generally, the higher potential for O_2 evolution of the anode, the weaker for the interaction of $M(OH)$ with the anode surface and the higher is the chemical reactivity toward organics oxidation [8]. As known, BDD anode is the most potent non-active anode due to the high potential for O_2 evolution, corrosion resistance and high chemical stability, thereby being considered the most ideal anode for EAOPs so far

[9,10]. However, the manufacture of BDD is very complicated and expensive, and still hardly to have a scale-up application [11,12]. Therefore, a cost-effective anode with high performance for organics degradation is urgently demanded, being one of the bottleneck for the application of EAOPs.

To lower the cost of anode fabrication, many researchers have

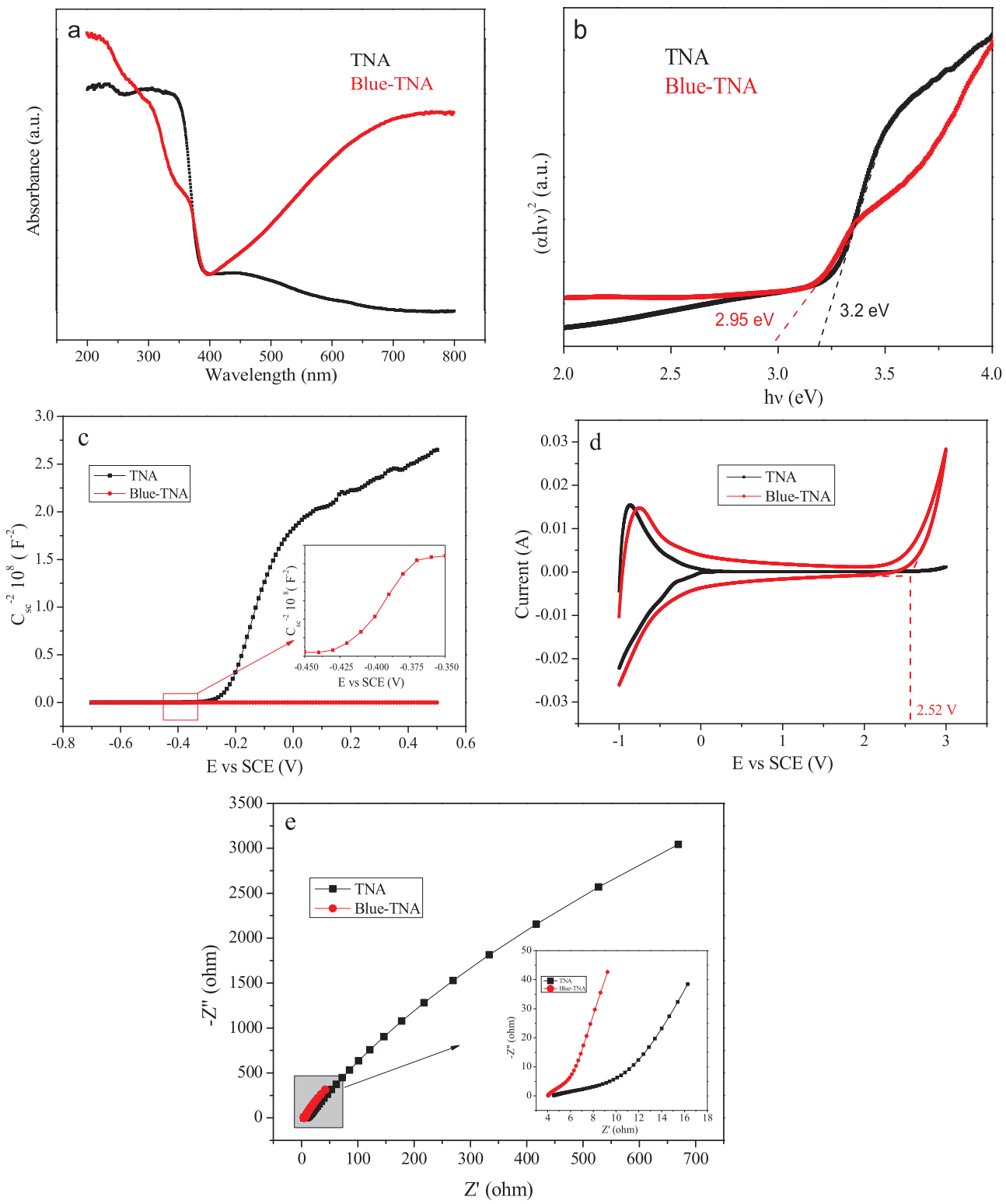


Fig. 3. (a) UV-vis curve (b) Tauc plot as a function of the photon energy (c) Mott – Schottky plots of TNA and Blue-TNA (d) CV (e) EIS.

attempted to modify commercialized Ti to be a cost-effective anode for wastewater treatment [13], especially TiO_2 nanotubes (TNA)/Ti has been reported to be a non-active anode [14]. However, the surface of Ti is easily oxidized to form a TiO_2 layer during anodic polarization, resulting in the poor conductivity which limits the application of TNA. To solve this problem, deposition metal oxide layer on TNA has been proposed [15,16]. Wang et al. [16] demonstrated that the introduction of $\text{SnO}_2\text{-Sb}$ on Ti/TNA resulted in a better performance for phenol

degradation. Later, many efforts on preparation of sub-stoichiometric TiO_2 electrode to improve anode conductivity have been made, particularly Ti_4O_7 anode has been developed for wastewater treatment due to its high conductivity and corrosion resistance [17–21]. However, the manufacture of this electrode was usually very harsh (e.g., requiring a high temperature over 800 °C), which would limit its application [22–24].

Recently, self-doped TiO_2 electrode has been found to improve the

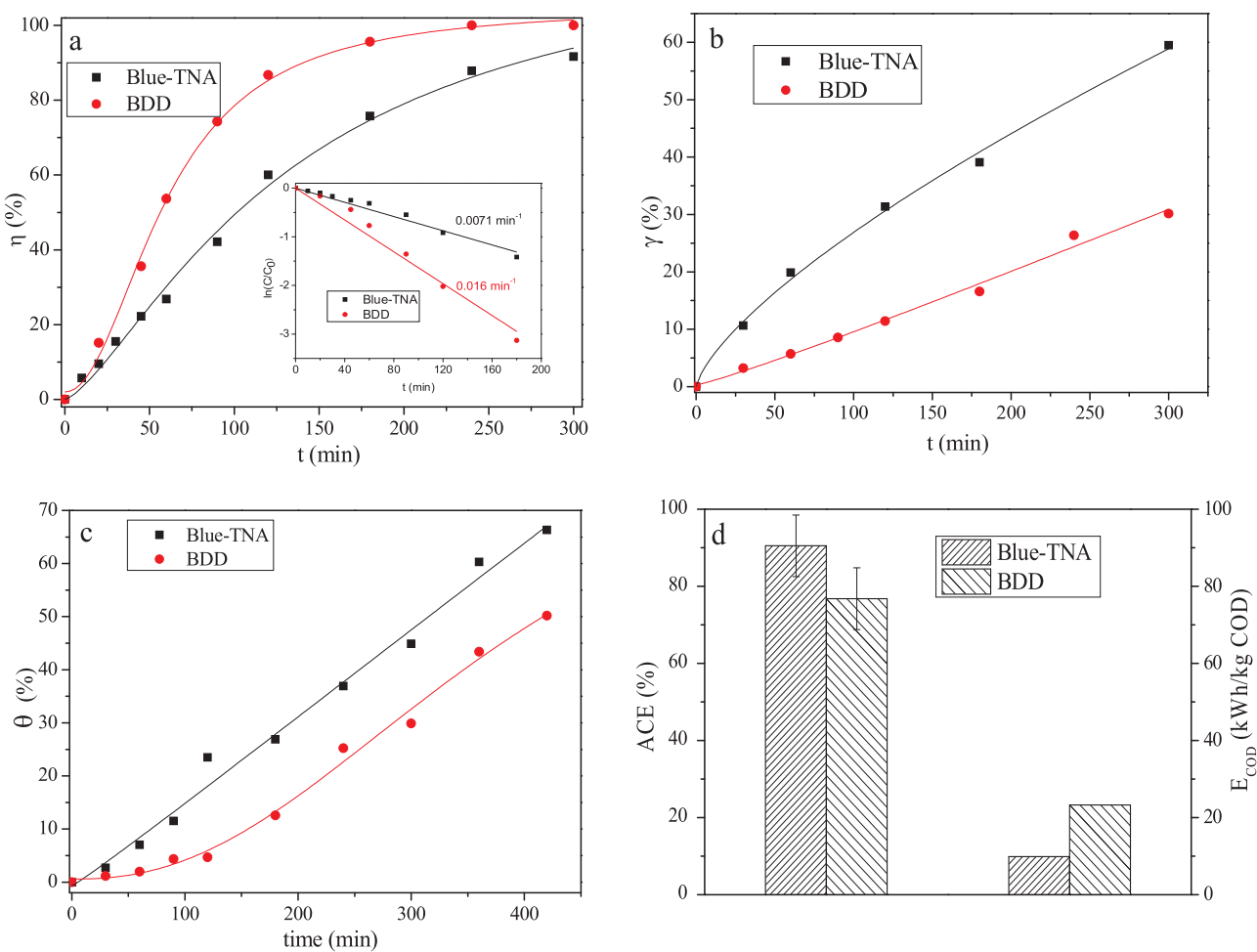


Fig. 4. Comparison between Blue-TNA and BDD. (a) phenol removal rate, (b) COD removal rate, (c) TOC removal rate, (d) ACE and E_{COD} of Blue-TNA and BDD. Conditions: phenol (100 mg/L), current density 2.5 mA/cm², pH 5, Na₂SO₄ 0.1 M.

conductivity of TiO₂ [25–27], in which Ti is anodically oxidized to TNA and after its electrochemical reduction the color of TNA turns from gray to blue, forming the so-called Blue-TNA [28]. At present, Blue-TNA is mainly used for super capacitor [25] and photo-degradation of organic pollutants [29,30], only very limited in anodic oxidation of pollutants such as salicylic acid [31], 4-chlorophenol and diclofenac [32]. Moreover, these literatures mainly focus on the optimization the preparation of Blue-TNA or the performance for the formation of Cl₂ or other oxidants or deposit some metal oxide like RuO₂ which result a very low O₂ over potential as 1.0 V vs. SCE [33–35]. The mechanism for anodic oxidation of organics, and how the parameters influencing the contribution of 'OH and SO₄²⁻ which are supposed to be existed in sulfate electrolyte, are still unclear due to the fact that in sulfate basing electrolyte at BDD anode, at high anodic potentials, a directed SO₄²⁻ production was possible by reaction (4) [36].



Herein, this work reported an excellent Blue-TNA electrochemically reduction in formic acid for organic pollutants degradation, using phenol as the target contaminant because it widely exists in many industrial effluents and has been used as model pollutant for different oxidation processes [37]. The purpose of this study was to: 1) characterize the anode morphology and properties by XRD, XPS, Mott-Schottky and electrochemical tests; 2) compare the performance and mechanism between BDD and Blue-TNA; 3) gain insight into the contribution of radicals to degradation upon different factors including current density, initial pH and Na₂SO₄ concentration; 4) explore the

application feasibility by investigation on the performance for different types of contaminants, the stability and superiority of Blue-TNA anode.

2. Experimental

2.1. Chemicals

Phenol (Beijing, Lideshi chemical technology Co., Ltd, > 97%) was used as the target organic pollutant. Methylene blue, sulfamethazine and coumarin was purchased from Aladdin (Shanghai). Tetracycline was purchased from Shanghai Yuanye biotechnology Co., Ltd. Na₂SO₄ (> 99.5%). Rhodamine B was obtained from Northern Tianyi chemical reagent factory. NaCl (> 99.8%) was purchased from Tianjin Guangfu technology development Co., Ltd. Sulfuric acid (H₂SO₄), sodium hydroxide (NaOH) (96%) and methanol (MeOH) (99.9%) were purchased from Tianjin Kemiou chemical reagent Co., Ltd. Phosphoric acid (85%) was obtained from Tianjin wind boat chemical reagents technology Co., Ltd. Benzoic acid was obtained from Macklin (Shanghai, China). Tert-butyl alcohol (TBA) (> 99.5%) was purchased from the sinopharm group chemical reagent Co., Ltd. (Shanghai, China). Benzoquinone (BQ) was obtained from Nine ding chemistry.

2.2. Blue-TNA preparation

TNA was obtained through a two-step anodization to achieve relatively stable and uniform structure. The first anodization was performed at 60 V for 1 h in the ethylene glycol electrolyte containing

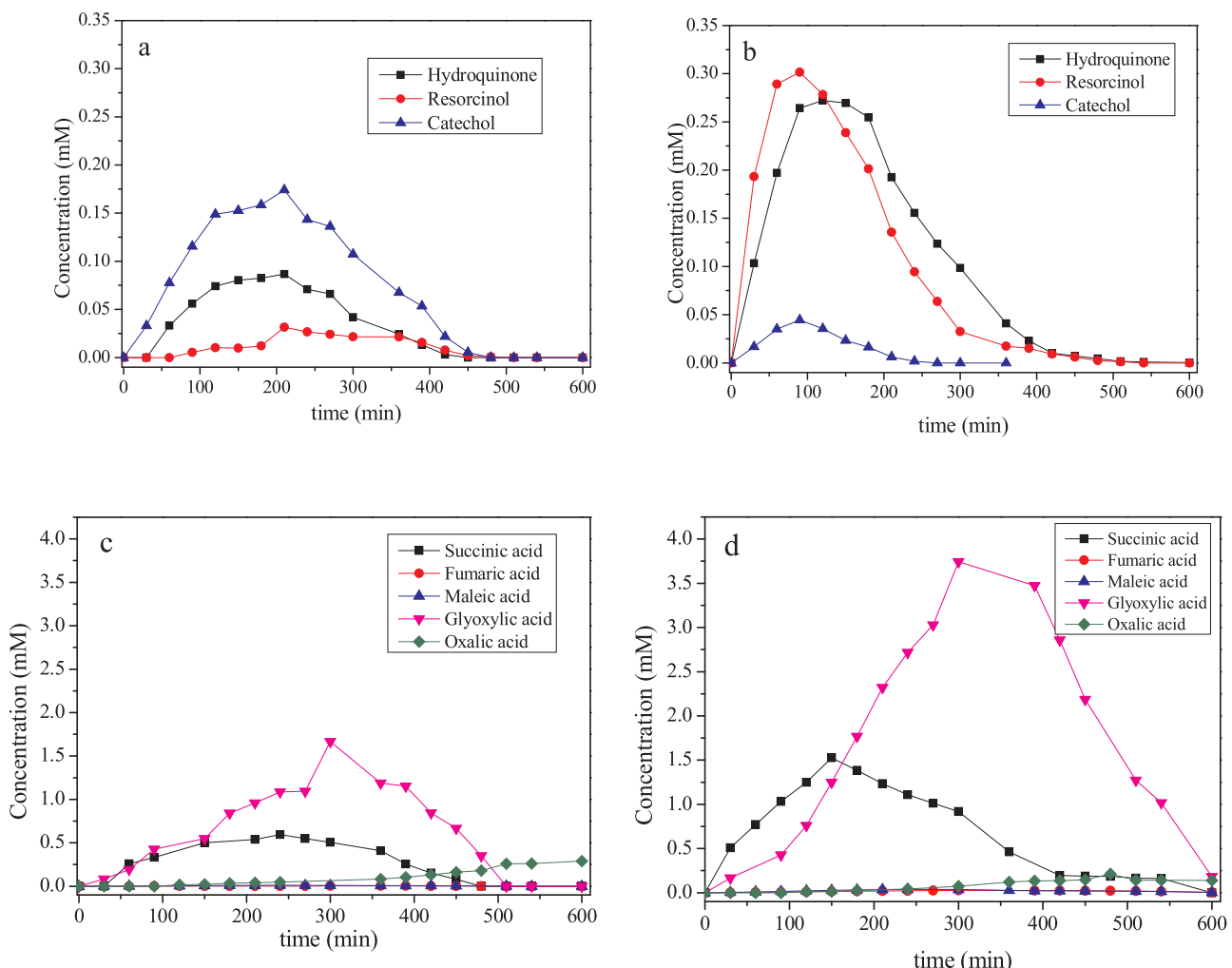


Fig. 5. Intermediates in (a) Blue-TNA system (b) BDD system; organic acid in (c) Blue-TNA system (d) BDD system, conditions: phenol (100 mg/L), current density 2.5 mA/cm², pH 5, Na₂SO₄ 0.1 M.

0.25 wt% NH₄F and 2 wt% distilled water in an undivided cell using Ti plate as the anode and Pt as the cathode. Then the obtained TNA was directly performed a second anodization at 60 V for 4 h in the ethylene glycol electrolyte containing 0.1 wt% NH₄F and 1 wt% distilled water. The as-formed TNA was annealed at 450 °C in air for 2 h with a ramp rate of 2 °C/min. In order to prepare the Blue-TNA, the formed TNA was electrochemically reduced at current density of 5 mA cm⁻² for 5 min in the solution of 10% formic acid (v : v) which could capture the oxygen in the TiO₂ crystal lattice and form the defects [38].

2.3. Physicochemical characterizations

The crystalline phases of TNA before and after electrochemical reduction were identified through X-ray Diffraction (XRD, Ultima IV Cu K α radiation). The morphologies of electrode were examined by Scanning Electron Microscopy (SEM, LEO-1530VP, Germany). The surface composition of TNA and Blue-TNA were obtained from X-ray Photoelectron Spectroscopy (XPS, Krato-ultra DLD, Shimadzu, Al K α radiation). Raman measurements were carried out using a Renishaw Modular Raman system at room temperature, and a 632.8 nm line from a He-Ne laser was used as the excitation laser.

2.4. Electrochemical tests

A single compartment cell with a three-electrode was employed, which included a working electrode (TNA or Blue-TNA, 1.5 × 2 cm²), a

stainless steel (SS, 2 × 2 cm²) counter electrode, and an Ag/AgCl (SCE) reference electrode. The electrode module was connected to a computer-controlled potentiostat (CHI 760D). The distance between anode and cathode was 1 cm and the supporting electrolyte was 0.1 M Na₂SO₄. Cyclic voltammetry (CV) data were collected in the potential range of -1 to +3.0 V (vs. SCE) at a scan rate of 100 mV/s. For electrochemical impedance spectroscopy (EIS) Nyquist plot, the potential bias was set at open circuit voltage (OCV) with a frequency range of 1 MHz to 0.01 Hz and alternating current (AC) voltage of 10 mV. The Mott - Schottky measurements were carried out at AC potential of 10 mV with a frequency of 1000 Hz in the potential range of -0.5 to +0.7 V (vs SCE). The diffuse reflectance UV - vis spectra was analyzed on a spectrophotometer (Shimadzu, UV-2600) with a wavelength scale of 200–800 nm.

2.5. Experimental setup

Anodic oxidation of phenol (100 mg/L), methylene blue (MB, 50 mg/L), 2,4-dichlorophenoxyacetic acid (2,4-D, 10 mg/L), sulfamethazine (SMT, 5 mg/L), *p*-nitrophenol (*p*NP, 10 mg/L), Rhodamine B (RhB, 50 mg/L) and tetracycline (TC, 10 mg/L) were performed in a beaker with the volume of 100 mL, continuously stirred by a magnetic bar. During the treatment, Blue-TNA and SS were the anode and cathode, respectively. In some experiments, initial pH (3–11) was adjusted with NaOH (1 mol/L) and H₂SO₄ (2 mol/L). For the quenching study, MeOH, BQ and TBA were employed as radical scavengers the

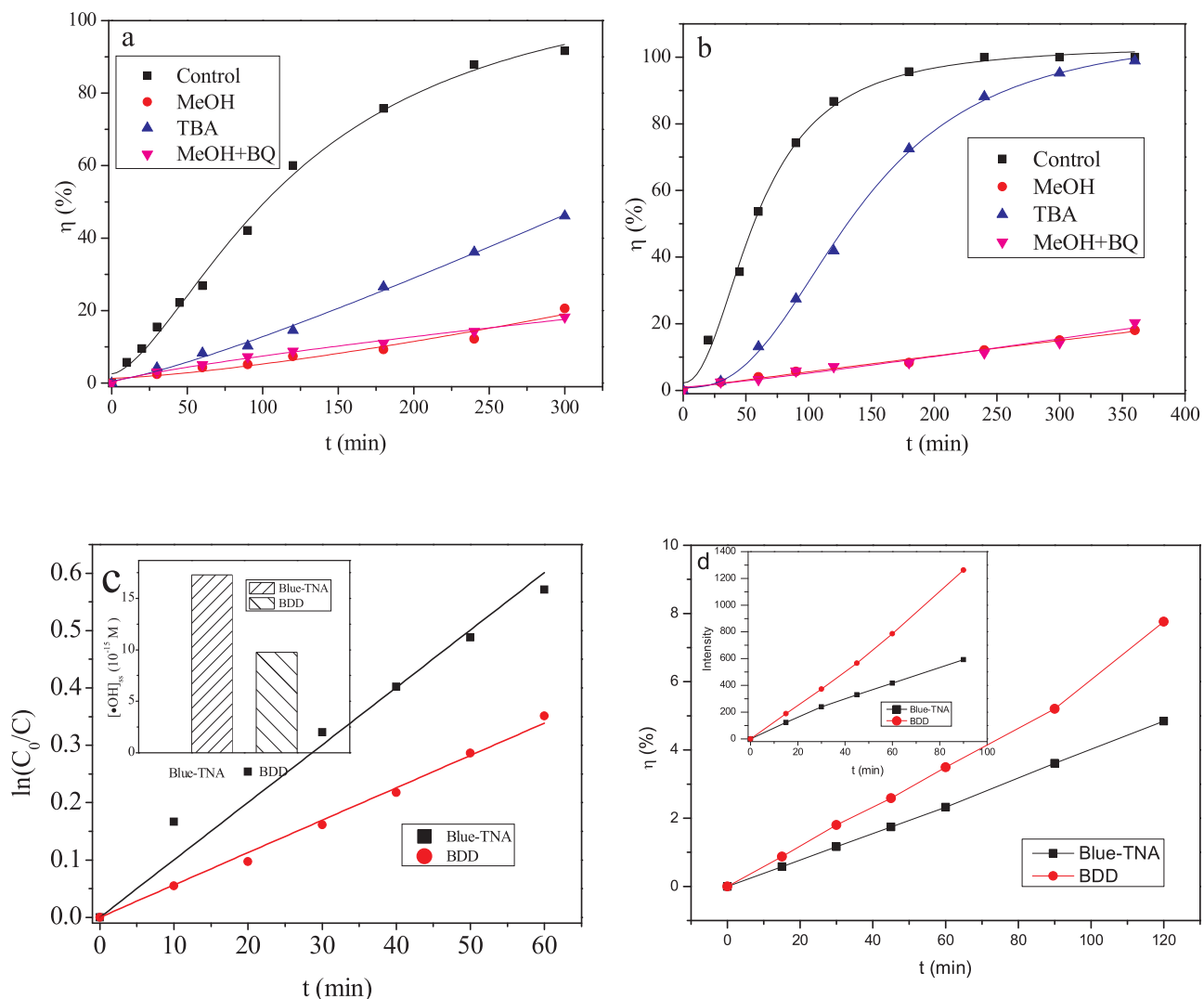


Fig. 6. Queching study on phenol degradation (a) Blue-TNA, (b) BDD. Conditions: phenol (100 mg L^{-1}), current density 2.5 mA/cm^2 , pH 5, Na_2SO_4 0.1 M. MeOH 5 M, TBA 2.2 M, BQ 10 mM. (c) $[\text{OH}]_{\text{ss}}$ estimated from 1 mM BA degradation in 30 mM NaClO_4 at 2.5 mA/cm^2 . (d) Degradation of coumarin, conditions: coumarin (2 mM), current density 2.5 mA/cm^2 , Na_2SO_4 0.1 M.

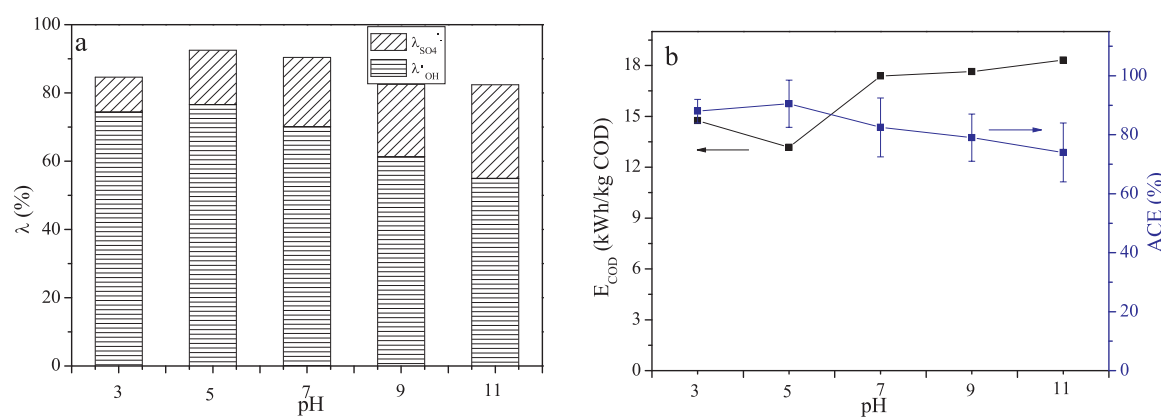


Fig. 7. (a) The effect of initial pH on the contribution of OH and SO_4^{2-} , (b) ACE and E_{COD} . Conditions: phenol (100 mg/L), current density 2.5 mA/cm^2 , Na_2SO_4 0.1 M.

concentration was 5 M, 2.2 M and 10 mM, respectively. Regularly, approximately 1.5 mL solution was sampled and filtered through a $0.45 \mu\text{m}$ membrane filter to be analyzed.

2.6. Analysis methods

The concentration of phenol, benzoic acid, 2,4-D and *p*-NP were determined by high performance liquid chromatography (U3000, ThermoFisher, America) with AcclaimTM 120 C18 column (3 μm ,

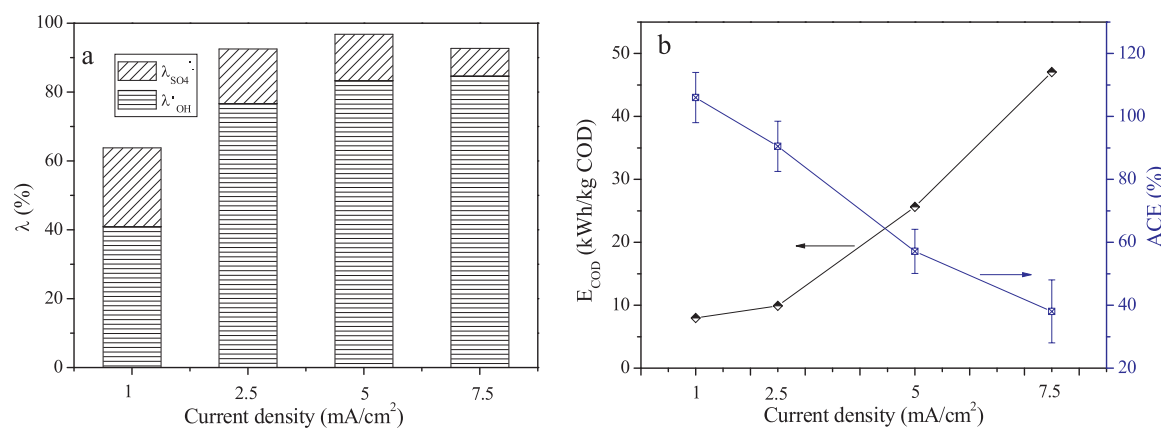


Fig. 8. (a) Effect of current density on the contribution of $\cdot\text{OH}$ and $\text{SO}_4^{\cdot-}$, (b) ACE and E_{COD} . Conditions: phenol (100 mg/L), pH 5, Na_2SO_4 0.1 M.

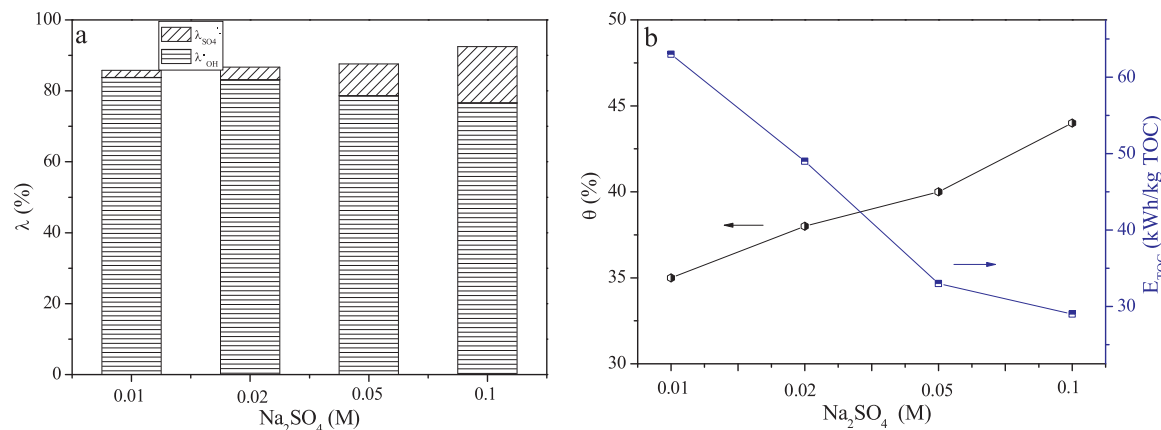


Fig. 9. (a) Effect of the concentration of Na_2SO_4 on the contribution of $\cdot\text{OH}$ and $\text{SO}_4^{\cdot-}$, (b) ACE and E_{COD} . Conditions: phenol (100 mg/L), current density 2.5 mA/cm², pH 5.

$\varphi 3.0 \times 100$ mm) at a flow rate of 0.3 mL/min coupled with a DAD detector. The mobile phase consisted of 60:38 (v/v) methanol/2% acetic acid. For the concentration of hydroquinone, catechol and resorcinol, the analytic method was the same as phenol except the flow rate was 0.2 mL/min. For the SMT and TC, the column was Acuity UPLC BEH C18 column (1.7 μm , $\varphi 2.1 \times 100$ mm) at a flow rate of 0.1 mL min^{-1} , the mobile phase consisted of 60:40 (v/v) methanol and water. The concentration of MB, RhB and coumarin were detected by the UV – vis spectrophotometer (Shimadzu, UV-2600) at wavelength of 486, 554 and 277 nm, respectively. The intensity of 7-hydroxycoumarin was monitored by fluorescence spectrophotometer (PerkinElmer LS-55, $\lambda_{\text{ex}} = 332$ nm and $\lambda_{\text{em}} = 460$ nm). The degradation efficiency (η %) of pollutants was calculated according to eq. (5).

$$\eta = \frac{C_0 - C_t}{C_0} \times 100\% \quad (5)$$

where, C_0 and C_t are the initial concentrations of contaminants (mg/L) concentration at reaction time t .

The concentration of oxalic acid, glyoxylic acid, fumaric acid, maleic acid and succinic acid were determined by high performance liquid chromatography (FL2200-2) with a Carbomix H-NP10 column (6.0 μm , $\varphi 7.8 \times 300$ mm) at a flow rate of 0.4 mL min^{-1} coupled with a UV detector at wavelength of 210 nm.

Hydroxyl radical production was measured by using benzoic acid (BA) as probe molecule. The quasi steady-state concentration of $\cdot\text{OH}$ ($[\cdot\text{OH}]_{\text{ss}}$) was estimated according to the previous study [24].

The chemical oxygen demand (COD) were measured using the dichromate digestion (Hach Method DRB200) and Total organic carbon (TOC) was determined using TOC-L (Shimadzu, Japan). The COD

removal (γ) and TOC removal (θ) were calculated according to eq. (6) and eq. (7), respectively.

$$\gamma = \frac{\text{COD}_0 - \text{COD}_t}{\text{COD}_0} \times 100\% \quad (6)$$

$$\theta = \frac{\text{TOC}_0 - \text{TOC}_t}{\text{TOC}_0} \times 100\% \quad (7)$$

where, COD_0 and COD_t are the initial concentrations of contaminants (mg/L) concentration at reaction time t . Where, TOC_0 and TOC_t are the initial concentrations of contaminants (mg/L) concentration at reaction time t .

The average current efficiency (ACE) was calculated from eq. (8).

$$\text{ACE} = \frac{FV}{8It} \frac{[\text{COD}_0 - \text{COD}_t]}{8It} \times 100\% \quad (8)$$

where COD_0 and COD_t are the initial COD (g/L) and the COD at time t , respectively, I the current intensity (A), F the Faraday constant (96,487 C/mol), t the time (s), V the volume of the electrolyte (L) and 8 derives from the equivalent mass of oxygen (g/eq).

The mineralization current efficiency (MCE) was calculated from eq. (9) [4].

$$\text{MCE} = \frac{nFV\Delta\text{TOC}}{4.32 \times 10^7 mIt} \times 100\% \quad (9)$$

where F is the Faraday constant (C/mol), V is the solution volume (L), 4.32×10^7 is a conversion factor (3600 s/h \times 12,000 mg of C/mol), m is the number of carbon atoms of contaminants and I is the applied current (A) and n is the number of electron consumed per molecule of contaminants.

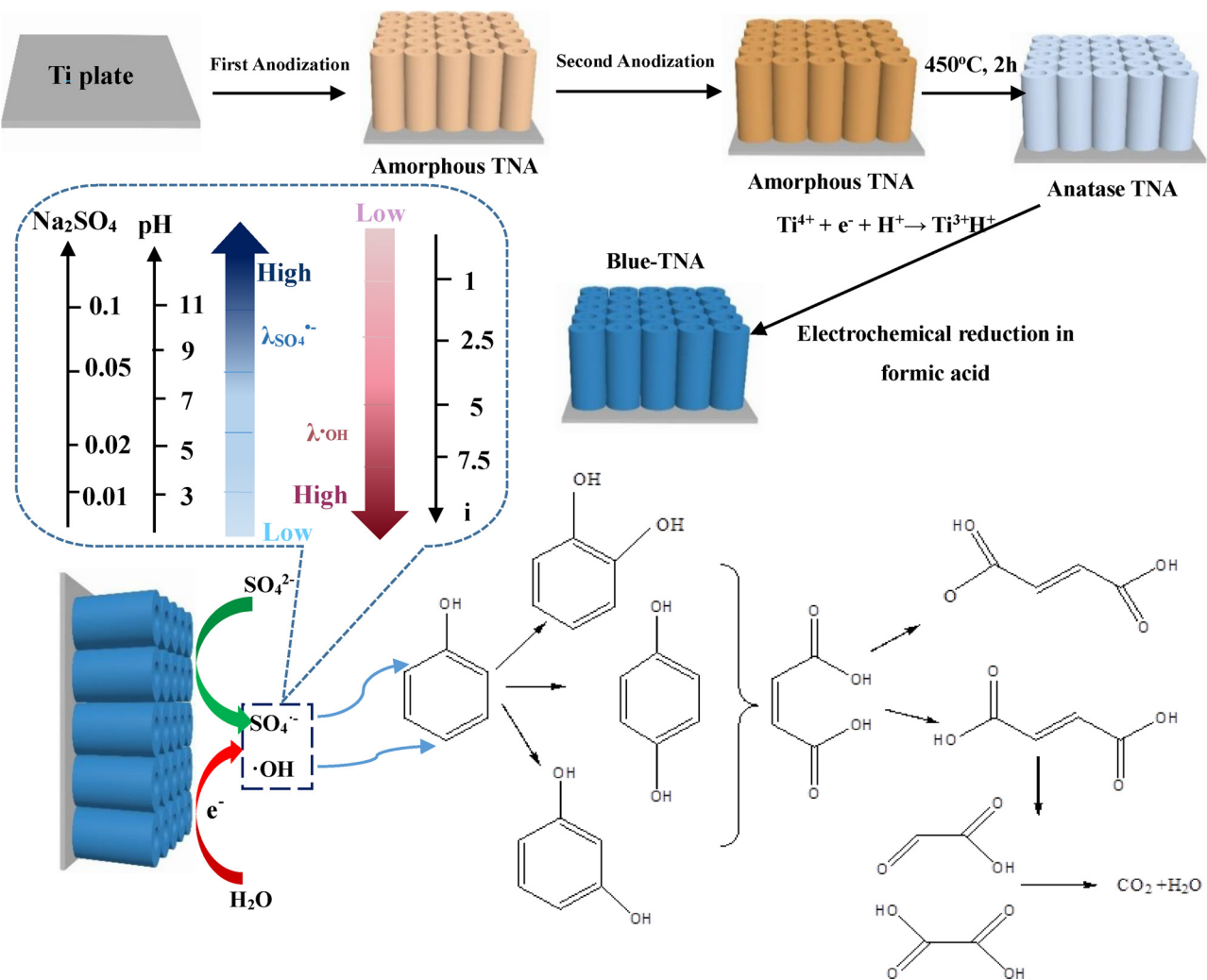


Fig. 10. The mechanism on Blue-TNA in sulfate electrolyte.

The energy consumption (E_{COD}) (kWh/kg COD) and (E_{TOC}) (kWh/kg TOC) were calculated according to eqs. (10–11) [1]:

$$E_{COD} = \frac{1000UIt}{(COD_0 - COD_t)V} \quad (10)$$

$$E_{TOC} = \frac{1000UIt}{(TOC_0 - TOC_t)V} \quad (11)$$

where, U is the cell voltage of the cell (V), I is the applied current (A), t is the reaction time (h), V is the volume of the cell, COD_0/TOC_0 and COD_t/TOC_t are the initial concentrations of COD/TOC (mg/L) and concentration at time t .

3. Results and discussion

3.1. Morphology and structure measurement

As shown in Fig. 1a, TNA was gray while after electrochemical reduction it turned to blue. Fig. 1b presents the surface morphology of TNA, observing the relatively uniform nanotubes, which remained intact after electrochemical reduction (Fig. S1). The NTA were well-aligned and organized into high-density and uniform arrays with the average tube length of around 15 μ m (inset Fig. 1b), tube wall of 54 nm and diameter around 100 nm. In summary, the morphology of TNA and Blue-TNA did not show a noticeable changes except the color, which was consistent with literature [34,39].

The corresponding XRD patterns are presented in Fig. 1c, both the TNA and Blue-TNA possess an anatase TiO_2 phase. However, the diffraction peak intensities of Blue-TNA were much weaker than TNA, which may be closely related to the formation of Ti^{3+} in the TiO_2 lattices [40,41]. To examine the crystallinity and microstructures of TNA and Blue-TNA, Raman scattering was conducted. As shown in Fig. 1d, the Raman active modes located at 144.4 cm^{-1} (Eg), 197.2 cm^{-1} (Eg), 396 cm^{-1} (B1g), 515 cm^{-1} (B1g), and 637.7 cm^{-1} (Eg) are both detected for TNA and Blue-TNA, indicating that the samples are composed of anatase [42,43]. Notably, the main Eg mode located at 144 cm^{-1} broadened and shifted toward higher wavenumber in Blue-TNA (insert Fig. 1d). This phenomenon was also observed in several recent studies [44,45], attributing to the formation of Ti^{3+} .

To further confirm the presence of Ti^{3+} sites in Blue-TNA, XPS studies were performed. The binding energies obtained were corrected for specimen charging by referencing the observed C1s binding energy to 284.5 eV. As shown in Fig. S2, the sharp peaks for Ti, O, and C elements were detected in TNA and Blue-TNA. No other peaks were detected, indicating that no impurity was introduced during reduction treatment. Fig. 2a shows the corresponding normalized Ti 2p core level XPS spectra. It was clearly that two broad peaks related to the characteristic $Ti 2p_{1/2}$ and $Ti 2p_{3/2}$ peaks were detected in TNA and Blue-TNA. Compared to TNA, the peaks of Blue-TNA in Fig. 2b displayed a redshift, suggesting that their different bonding environments. After fitting, the peaks centered at 458.5 and 464.3 eV could be assigned to Ti^{4+} , whereas the peak at low binding energy of 457.9 and 463.6 eV

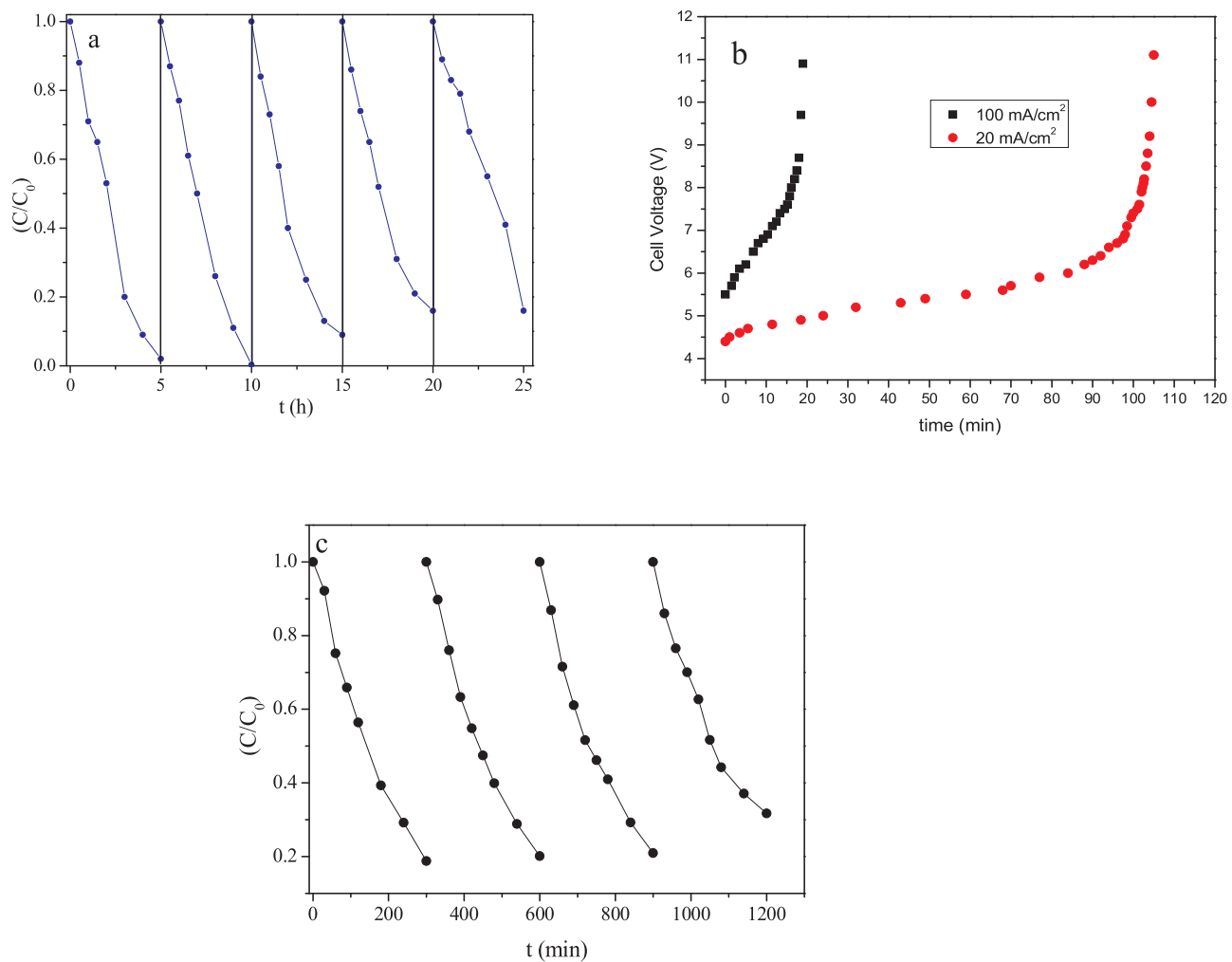


Fig. 11. (a) Phenol degradation and for 5 consecutive experiments using Blue-TNA. Conditions: phenol (100 mg/L), current density 2.5 mA/cm^2 , pH 5, Na_2SO_4 0.1 M. (b) Accelerated lifetime test of Blue-TNA at 20 and 100 mA/cm^2 . Electrolyte is 1 M NaClO_4 (c) Phenol degradation on Blue-TNA after regeneration.

could be attributed to Ti^{3+} [26,44]. The abundance of Ti^{3+} detected in Blue-TNA was calculated to be 82%, whereas in TNA was 22%. This result indicated that more Ti^{3+} sites were indeed created in Blue-TNA during electrochemical reduction [35,45].

3.2. Band structure analysis and electrochemical characterization

According to the above results, some Ti^{4+} reduce to Ti^{3+} during electrochemical reduction. The loss of charge was due to the H^+ intercalation [28]. UV – vis reflectance spectra was used to study the absorbance and bandgap. As described in Fig. 3a, after reduction Blue-TNA had a stronger infrared adsorption than TNA, and the band gap of Blue-TNA (2.97 eV) was comparable to other self-doping TNA as depicted in Fig. 3b, which was lower than the TNA (3.2 eV). This strong absorption and narrow band gap was due to the surface disorders and existence of Ti^{3+} defects, which induced a continuous vacancy band of electronic states [46].

Mott-Schottky plots were measured in TNA and Blue-TNA. As shown in Fig. 3c, the slope of the liner part was positive, indicating that the type of Blue-TNA was still the n-type semiconductor characteristics [33]. The values of E_{fb} were estimated to be -0.32 V and -0.44 V vs. SCE for the TNA and Blue-TNA, respectively. The negative shift of E_{fb} after reduction suggested a same shift of the Fermi level due to the formation of Ti^{3+} that facilitated the charge separation at the semiconductor and electrolyte interface [47,48]. The donor densities (N_D) calculated from the Mott-Schottky eq. (12) [49] were up to 1.0×10^{20} and

$5.8 \times 10^{25} \text{ cm}^{-3}$ for the TNA and Blue-TNA, respectively.

$$\frac{1}{C_{sc}^2} = \left[\frac{2}{e\epsilon_0 \epsilon N_D} \right] \left[(E_s - E_{fb}) - \frac{KT}{e} \right] \quad (12)$$

where C_{sc} is the space charge capacitance (F/cm^2); e is elementary charge ($1.602 \times 10^{-19} \text{ C}$); ϵ is the relative dielectric constant of electrode material (48 for anatase TNA; assumed to be identical for Blue-TNA), ϵ_0 is the permittivity of vacuum ($8.85 \times 10^{-12} \text{ N}^{-1} \text{ C}^2/\text{m}^2$); E_s is the applied potential (V); E_{fb} is the flat band potential (V); k is the Boltzmann's constant ($1.38 \times 10^{-23} \text{ J/K}$), and T is the absolute temperature (K).

An increased value of N_D in semiconductors improved the charge conductivity. The electrical property characterization confirmed that the Blue-TNA had a better electrical conductivity than TNA, which accelerated the electron transfer and suppressed the recombination of electrons and holes [28,44]. The better electrical conductivity of Blue-TNA was also confirmed by the curve of CV and EIS which exhibited a high O_2 over-potential of 2.52 V (vs SCE), and a much lower resistance of R_{ct} and R_d with the value of 32Ω and 682Ω , respectively, compared with the TNA of the resistance of R_{ct} and R_d (333Ω and 2848Ω).

3.3. Comparison of anodic oxidation of phenol using Blue-TNA and BDD anode

Anode material is important for anodic oxidation, thus the anodic oxidation of phenol was compared with BDD, which was reported to be

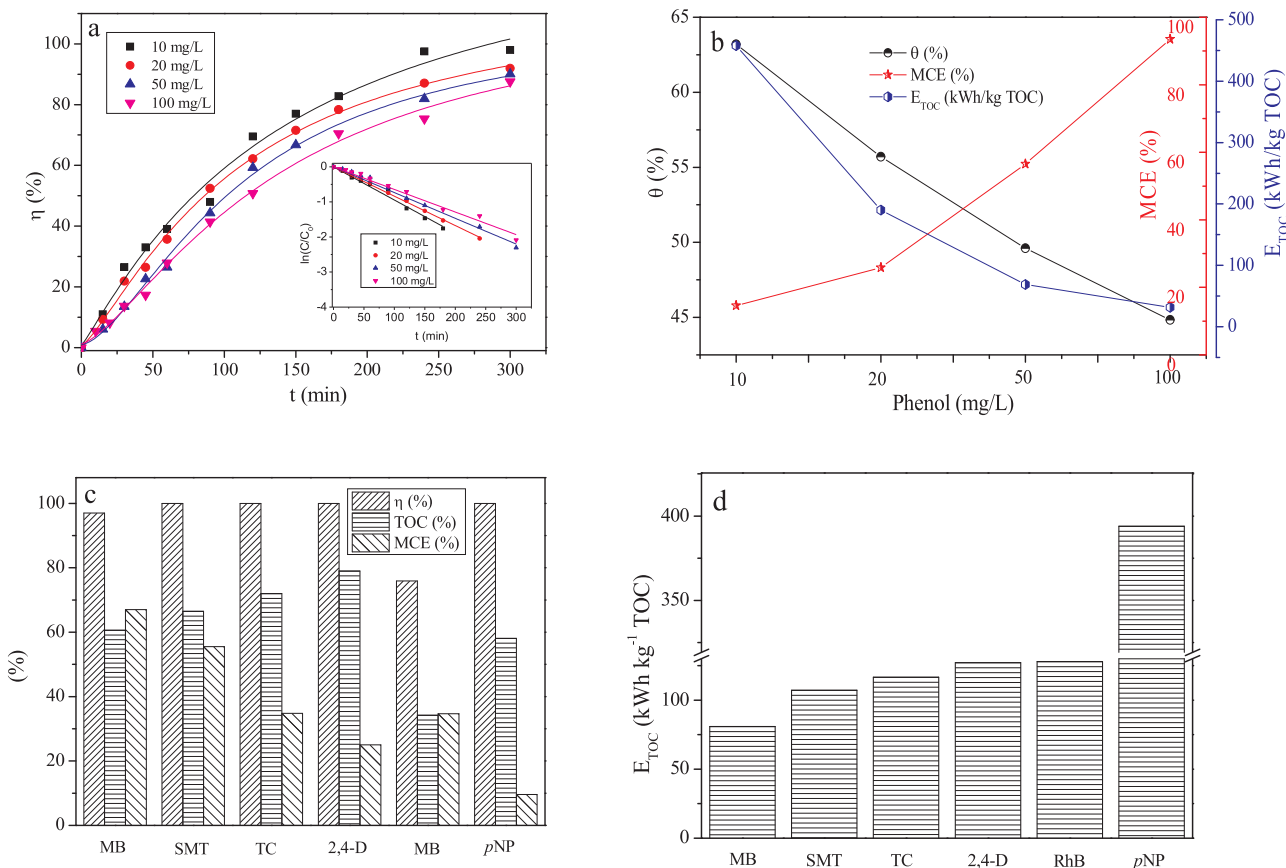


Fig. 12. (a) the effect of initial phenol concentration on its degradation (b) the value of TOC removal, MCE and E_{TOC} (c) The value of TOC removal, MCE and removal efficiency of different contaminants on Blue-TNA anode, (d) energy consumption of different contaminants. Conditions: current density 2.5 mA/cm², Na₂SO₄ 0.1 M.

the most efficient anode for organics removal [49]. Fig. 4a shows the removal of phenol on BDD and Blue-TNA at 2.5 mA/cm² in 0.1 M Na₂SO₄ at pH 5, observing the complete removal of phenol on BDD at 240 min while only 87% on Blue-TNA. The degradation rate constant on BDD was two times of the one obtained on Blue-TNA (insert Fig. 4a). However, the removal of TOC and COD on Blue-TNA were 44% and 59% at 300 min, respectively, which was much higher than that on BDD (29% and 30% as shown in Fig. 4b and 4c). Therefore, the ACE on Blue-TNA (90.5%) was higher than that on BDD (76.8%) with a lower E_{COD} of only 9.9 kWh/(kg COD) compared with the value of 23.3 kWh/(kg COD) on BDD (Fig. 4d).

To discover the possible reason for the different performance on phenol removal and COD, TOC removal, the degradation intermediates and carboxylic acids were measured. As depicted in Fig. 5a and 5b, the main intermediates during phenol degradation was hydroquinone, catechol and resorcinol. The concentration of hydroquinone and resorcinol on BDD were much higher than that on Blue-TNA. The maximum concentration of hydroquinone and resorcinol on BDD were 0.27 and 0.30 mM, respectively, while on Blue-TNA they were only 0.086 and 0.031 mM. For catechol, the maximum concentration on BDD was 0.045 mM howbeit on Blue-TNA was 0.17 mM, which was a bit higher than that on BDD. However, due to the fact that the same molecular formula of hydroquinone, catechol and resorcinol (C₆H₆O₂), the same amount had the equal COD and TOC value.

The mainly detected carboxylic acids were oxalic acid, glyoxylic acid, fumaric acid, maleic acid and succinic acid. As shown in Fig. 5c and 5d, glyoxylic acid showed the highest concentration among the carboxylic acids on both systems, however, it peaked on BDD about two times that on Blue-TNA. Also, the concentrations of the rest carboxylic acids on Blue-TNA were much lower than on BDD.

To investigate the possible mechanism about the low concentration

of intermediates and organic acids on Blue-TNA, a series of quencher studies were performed. Due to the fact that MeOH had a comparable rate constant with 'OH ($9.7 \times 10^8 \text{ M}^{-1} \text{ s}^{-1}$) and SO₄²⁻ ($1.0 \times 10^7 \text{ M}^{-1} \text{ s}^{-1}$), while TBA had a rate of $3.8-7.6 \times 10^8 \text{ M}^{-1} \text{ s}^{-1}$ with 'OH whereas only $4.0-9.1 \times 10^5 \text{ M}^{-1} \text{ s}^{-1}$ with SO₄²⁻. Hence MeOH was the scavenger for SO₄²⁻ and 'OH, and TBA was supposed to scavenge only 'OH and benzoquinone (BQ) was O₂²⁻ capture [50,51]. As shown in Fig. 6a, when added MeOH into the solution, the removal of phenol within 5 h was only 20%. Moreover, when added TBA the removal of phenol within 5 h was about 50%, but when MeOH and BQ were added together, the removal of phenol did not show a significant change, indicating that the degradation of phenol was the collective effect of 'OH and SO₄²⁻ without the role of O₂²⁻. For the quencher study on BDD (Fig. 6b), when added MeOH only 18% phenol was degraded, and added BQ together also had the same result, while added TBA the phenol was total removed possibly due to sulfate radical oxidation on BDD [52]. Chosen benzoic acid as the 'OH probes, a higher [OH]_{ss} ($1.7 \times 10^{-14} \text{ M}$) on Blue-TNA was obtained than on BDD ($9.8 \times 10^{-15} \text{ M}$), indicating anodic oxidation on Blue-TNA had a higher 'OH production [28].

The relative contribution of 'OH and SO₄²⁻ was calculated according to the previous study [53], according to the eqs.(13-14). For Blue-TNA the contribution of 'OH was 76.6% and only 15.9% for the SO₄²⁻, however, for BDD, the contribution of 'OH was 52.3% and 44.1% for SO₄²⁻. This indicated that for Blue-TNA the mainly reaction radical was 'OH under this condition, while for BDD, both 'OH and SO₄²⁻ play an important role for phenol degradation.

$$\lambda_{\text{OH}} = \frac{k - k_{\text{TBA}}}{k} \times 100\% \quad (13)$$

Table 1
Performance comparison with literatures.

Methods	Anode	Conditions	i (mA/cm ²)	η (%)	γ (%)	E _{COD} (kWh/kg COD)	Ref.
Pulse-BDD anode system	BDD/Ni (24 cm ²)	COD ₀ 500 mg/L, f 110 Hz, pulse duty cycle 10, t 45 min	6	—	43.7	34.1	[40]
Ultrasound -electrochemical oxidation	BDD/Si (24 cm ²)	sound frequency 33 kHz, power 50 W, COD ₀ 531 mg/L, pH 3, t 192 min	20	—	100	123	[60]
Anodic oxidation	Pt- and Ru-doped Ti/SnO ₂ -Sb (20 cm ²)	phenol 1000 mg/L, 0.5 M NaOH, t 1440 min	10	78	17	47	[61]
Anodic oxidation	Ti/SnO ₂ -Sb ₂ O ₃ -CNT/PbO ₂ (15 cm ²)	phenol 100 mg/L, 0.25 M Na ₂ SO ₄ , pH 7, t 300 min	30	94	95	250	[62]
Anodic oxidation	BDD/Si (3 cm ²)	phenol 100 mg/L, 0.1 M Na ₂ SO ₄ , pH 5, t 300 min	2.5	100	30	23.3	This work
Anodic oxidation	Blue-TNA (3 cm ²)	phenol 100 mg/L, 0.1 M Na ₂ SO ₄ , pH 5, t 300 min	2.5	97	60	9.9	This work
Anodic oxidation	BDD/Si (3 cm ²)	2,4-D 230 mg/L, 0.05 M Na ₂ SO ₄ , pH 3, t 180 min	33.3	—	57 [*]	—	[63]
Anodic oxidation	BDD (3 cm ²)	SMT 193 mg/L, 0.05 M Na ₂ SO ₄ , pH 3, t 360 min	33.3	—	70 [*]	—	[64]
Anodic oxidation	Ti/Pt (25 cm ²)	pNP 100 mg/L, 7 mM Na ₂ SO ₄ , pH 2, t 300 min	30	92	22 [*]	—	[65]
Anodic oxidation	Ti/SnO ₂ -Sb (75 cm ²)	RhB 50 mg/L, 0.01 M Na ₂ SO ₄ , pH 4.5, t 30 min	20	99.9	86.7 [*]	—	[66]
Anodic oxidation	Ti/Pt (15 cm ²)	MB 50 mg/L, 0.5 M H ₂ SO ₄ , pH 1, t 900 min	10	100	30 [*]	—	[67]

Note: ^{*} TOC removal.

$$\lambda_{SO_4^{2-}} = \frac{k_{MeOH} - k_{TBA}}{k} \times 100\% \quad (14)$$

where k was the rate constant of phenol degradation without addition of scavenger, k_{TBA} was the rate constant with addition of TBA, k_{MeOH} was the rate constant with addition of MeOH.

Normally, two kinds of 'OH were existed in anodic oxidation, the free 'OH and surface 'OH. Coumarin was an 'OH probe by forming an 'OH adduct product 7-hydroxycoumarin, and Bejan et al. [54] revealed that 7-hydroxycoumarin which could oxidized by 'OH, as listed in Fig. 6d, when the same amount of coumarin was removed, the less quantity of 7-hydroxycoumarin was observed in Blue-TNA system, which meant that 7-hydroxycoumarin was easily to further oxidation on Blue-TNA anode, according to the previous study the 'OH generated on BDD was free 'OH, in BDD system, the concentration of coumarin was much higher than 7-hydroxycoumarin, herein, coumarin was preferentially oxidized. For Blue-TNA system, the production of 'OH was higher than BDD, so if the 'OH was free, more coumarin should be oxidized and had higher 7-hydroxycoumarin, however, the fact was converse, therefore, the 'OH on Blue-TNA was more likely surface 'OH, which could had a higher TOC and COD removal while low phenol degradation.

3.4. Contribution of 'OH and SO₄²⁻ at different conditions

3.4.1. Initial pH

From section 3.3, it was concluded that both 'OH and SO₄²⁻ played a role for phenol degradation on Blue-TNA. On the other hand, 'OH and SO₄²⁻ display a different reactivity at different initial pH [55]. Therefore, it is necessary to investigate the contribution of 'OH and SO₄²⁻ at different initial pH under the condition of 2.5 mA/cm² in 0.1 M Na₂SO₄. The degradation rate constant decreased from 0.0060 at pH 3 to 0.0039 min⁻¹ at pH 11, while at pH 5 the biggest rate constant of 0.0071 min⁻¹ was obtained. When added TBA into the solution, the degradation rate constant increased from 0.0015 to 0.0018 min⁻¹ as pH increased from 3 to 11 (Tab. S1). As shown in Fig. 7a, when the initial pH increased from 3 to 11, the contribution of 'OH decreased from 74.4% to 55%, the contribution of SO₄²⁻ increased from 10.2% to 27.4%. This might be due to the fact that at acidic condition 'OH exhibited stronger oxidation ability than at alkaline condition. Besides, owing to acid-catalyzed, electro-generated SO₄²⁻ easily react with other radicals. At alkaline condition, 'OH showed a weak reactivity, while SO₄²⁻ displayed a better oxidizing ability. However, SO₄²⁻ could be converted to 'OH through eq. (15) with a rate constant of 6.5 × 10⁷ M⁻¹ s⁻¹ and 'OH shown a lower reactivity at alkaline condition [56]. Therefore, when the initial pH was among 3 and 7, the removal of phenol was almost the same (Fig. S2a), however, when the initial pH was 9 and 11, the removal of phenol and COD were slightly slower than that in the acidic solution (Fig. S2b). The same results of the E_{COD} and ACE were also obtained (Fig. 7b), when pH was among 3–7, the value of E_{COD} was below 17 kWh/(kg COD) with the ACE value over 80%, while when pH was 9 and 11, the E_{COD} was 17.6, 18.3 kWh/kg COD, the ACE value was 79% and 74%, respectively, which was inferior to that at the low pH. This meant that for phenol decay on Blue-TNA the main radical was 'OH at pH 3–11 due to the over 55% contribution.



3.4.2. Effect of current density

Current density is an essential parameter for the generation of 'OH. The degradation of phenol was enhanced with the increasing current density (Fig. S3a). The rate constant increased from 0.0020 to 0.015 min⁻¹ when the current density increased from 1 to 7.5 mA cm⁻², while added TBA the rate constant increased from 0.0012 to 0.0024 min⁻¹ (Tab. S2). As shown in Fig. 8a, increasing current density from 1 to 7.5 mA cm⁻², the contribution of 'OH enhanced from 40.9% to

84.6%, while the contribution of $\text{SO}_4^{\cdot-}$ decreased from 22.8% to 8.1%. This was due to high current density usually produce more $\cdot\text{OH}$ and $\text{SO}_4^{\cdot-}$, and $\cdot\text{OH}$ could react with $\text{SO}_4^{\cdot-}$ to form $\text{S}_2\text{O}_8^{\cdot2-}$ which had a low activity. Additionally, $\text{SO}_4^{\cdot-}$ could also be converted to $\cdot\text{OH}$ by reaction (16) which enhance the $\cdot\text{OH}$ contribution [57]. On the other hand, high current density normally enhance the side reactions such as oxygen evolution. Blue-TNA possess the best COD removal at the current density of 2.5 mA/cm^2 (Fig. S3b). Further increase the current density to 5 and 7.5 mA/cm^2 , a lower COD removal was observed, owing to relatively larger percentage of energy consumed by the oxidation of water [58]. Increasing the current density to 7.5 mA/cm^2 , the E_{COD} increased from 7.9 to 47 kW h/kg COD with the ACE significantly decreased to 38.6% (Fig. 8b).



3.4.3. Effect of Na_2SO_4 concentration

Na_2SO_4 concentration has influence on the electrolyte conductivity as well as the generation of $\text{SO}_4^{\cdot-}$. The phenol degradation rate constant increased from 0.0049 to 0.0071 min^{-1} when Na_2SO_4 concentration increased from 0.01 to 0.1 M at 2.5 mA/cm^2 with the solution pH of 5, and the rate constant increased from 8.0×10^{-4} to 0.0017 min^{-1} as added TBA (rate constant in Tab. S3). As illustrated in Fig. 9a, when Na_2SO_4 concentration increased from 0.01 to 0.1 M, the contribution of $\text{SO}_4^{\cdot-}$ increased from 2% to 15.9%, and the contribution of $\cdot\text{OH}$ decreased from 83.8% to 76.6%. These results were not surprised, since a high Na_2SO_4 concentration could produce more $\text{SO}_4^{\cdot-}$ at anode, while more $\text{SO}_4^{\cdot2-}$ could act as a $\cdot\text{OH}$ scavenger to consume the amount of $\cdot\text{OH}$ [50]. Besides, when the same current density was applied, a low Na_2SO_4 concentration needed a large cell voltage which could generate more $\cdot\text{OH}$. Therefore, the removal of phenol and rate constant increased from 56% to 75% (Fig. S4a), respectively, when the Na_2SO_4 concentration decreased from 0.1 to 0.01 M. However, the energy consumption increased from 27 to 63 kW h/kg TOC , with the TOC removal decreased from 44% to 34% (Fig. 9b). Anodic oxidation pathways have been explained by the role of $\cdot\text{OH}$ and other reactive oxygen species, while the participation of sulfate radical species has been largely neglected. This study imply that sulfate species cannot be considered as inert in electrochemical treatment even at low current density. Therefore, Blue-TNA was a promising anode for treatment of wastewater containing the sulfate-based solutions.

From the above results it could be concluded that phenol degradation on Blue-TNA was the comprehensive effect of $\cdot\text{OH}$ and $\text{SO}_4^{\cdot-}$. As denoted in Fig. 10, after two step anodization, the color of formed TNA was brown, annealed at 450°C for 2 h it turned to gray, after reduction it was blue. This anode had an excellent $\cdot\text{OH}$ and $\text{SO}_4^{\cdot-}$ production due to the formation of Ti^{3+} . Besides, low current density, high initial pH and high Na_2SO_4 favored for the contribution of $\text{SO}_4^{\cdot-}$. Once contaminants like phenol existed in the solution, $\cdot\text{OH}$ and $\text{SO}_4^{\cdot-}$ generated on the anode would destroy phenol to form the intermediates of hydroquinone, catechol and resorcinol, and form the carboxylic acids including oxalic acid, glyoxylic acid, fumaric acid, maleic acid and succinic acid then up to mineralization.

3.5. Electrode stability measurement and accelerated lifetime test

Blue-NTA has shown excellent electro-oxidation capability of phenol. In the present study, 5 cycles were conducted using 100 mL phenol solution each time. All the electro-oxidation experiments were carried out at the current density of 2.5 mA/cm^2 for 5 h in 0.1 M Na_2SO_4 solution. Fig. 11a compares phenol degradations for 5 cycles. After 5 cycles experiments, the removal of phenol was 85% compared to the first cycle it was reduced 15% which meant that Blue-NTA had a reasonable stability electrochemical performance. Geng et al. [22] revealed that Ti_4O_7 electrode that obtaining at 850°C for 30 min under

hydrogen atmosphere for phenol degradation could achieve 6 cycles stable performance within each reaction time of 2 h, while the volume was only 20 mL when compared to this study that treating 100 mL solution for 5 h each time.

As depicted in Fig. 11b the lifetime of Blue-NTA was determined to be 105 min at 20 mA/cm^2 and 20 min at 100 mA/cm^2 , which could be calculated the service life at 2.5 mA cm^{-2} was about 106 h (the calculation was listed in the support information). Thus, the deactivation of the Blue-NTA could be ascribed to the oxidation of Ti^{3+} at high applied anodic potentials, which could be confirmed from the CV curve (Fig. S6). TNA had the lowest current response due to the poor conductivity, when reduced in formic acid the conductivity was improved due to the formation of Ti^{3+} , after 5 cycles experiments, the current response was lower than the fresh one while higher than TNA electrode. The service life was low for industrial application, while Yang et al. [58] indicated that when induced cobalt the service life was over 200 h at 10 mA/cm^2 , but the oxygen evolution potential was only 1.7 V vs. RHE , therefore, it was promising to prepare a stable anode with high oxygen evolution potential. For this study, when using the deactivation electrode reduction in the formic acid once more, the new electrode could achieve a 4 cycles excellent performance in Fig. 11c, which due to the better current response than the aged one while had a comparable current response with the fresh one (Fig. S6).

3.6. Degradation of different contaminants on Blue-TNA anode

Different initial phenol concentration (10–100 mg/L) on its degradation was studied to explore the superiority of Blue-TNA. As displayed in Fig. 11a and b, the phenol and TOC removal decreased as the initial phenol concentration increased from 10 to 100 mg/L, with the degradation rate constant decreased from 0.0095 to 0.0071 min^{-1} . However, the MCE increased from 14.6% to 93.5%, with the accordingly energy consumption decreased from 458 to 31 kW h/kg TOC (Fig. 11b). This results could be explained by the diffusion control [59]. The type of $\cdot\text{OH}$ on Blue-TNA anode was surface absorbed $\cdot\text{OH}$, therefore, at the low initial concentration, more phenol and intermediates could degrade at the anode surface, at the high initial phenol concentration, more phenol could transferred to the anode surface which prevent the contact between intermediates and active sites. Normally, high MCE could be achieved for high initial concentration of pollutants. Moreover, the actual TOC removal amount was found to be increased with the initial phenol concentration. This indicated that anodic oxidation on Blue-TNA would be a much more cost-effective for higher concentration pollutants.

In order to investigate the capability of Blue-TNA for different types of pollutants, several contaminants including phenol, MB, 2,4-D, *p*NP, SMT, RhB and TC were selected to degrade on Blue-TNA anode (Fig. 12). Fig. S7 presents the removal of different contaminants could achieve 100% within 240 min, except the RhB (72%). Table 1 lists the comparison on removal performance and energy consumption with the literatures using anodic oxidation and combined methods for different contaminants. In literatures for phenol degradation, the minimum E_{COD} was 43.1 kW h/kg COD in the pulse-BDD anode system [40], for the combined methods like the ultrasounds- electrochemical the E_{COD} was about 123 kW h/kg COD [60], for the anode based on the titanium, such as Pt-Ru-doped $\text{Ti/SnO}_2\text{-Sb}$ and porous $\text{Ti/SnO}_2\text{-Sb}_2\text{O}_3\text{/CNT/PbO}_2$ [61,62], the E_{COD} was over 50 even to 250 kW h/kg COD . However, the E_{COD} on Blue-TNA was only 9.9 kW h/kg COD in the present work. TOC removal, MCE and E_{TOC} of 2,4-D were 79%, 25% and $127.2 \text{ kW h/kg TOC}$, respectively (Fig. 12c and d). The performance was better than that on the BDD anode at current 33.3 mA/cm^2 , achieving a 57% TOC removal at 240 min with a low MCE of 16% [63].

For the degradation of SMT, El-Ghemy et al. [64] used BDD anode to destroy it under current density of 33.3 mA/cm^2 , the TOC removal at 4 h was about 70% with the MCE of 11%. In this study, the TOC removal, MCE and E_{TOC} were 66.5%, 55.5% and $107.2 \text{ kW h/kg TOC}$,

respectively. When comes to the *p*NP, the TOC removal (58%) on Blue-TNA was better than the value obtained on Pt (22% at 4 h) [65]. For the dyes of Rhodamine B, when using the Ti/SnO₂-Sb anode, though the removal of TOC (86.7%) was higher than the one obtained in this work (34%), while the O₂ over potential was low usually exhibit unsatisfied current efficiency [66]. In terms of MB, when using Ti/Pt anode, only 30% TOC could be removed at 900 min at 10 mA/cm² [67], but for Blue-TNA anode MB could be completely removed with a high MCE of 67% and a low energy consumption of 80.9 kW h/(kg TOC). Therefore, Blue-TNA was an efficient anode for contaminants removal even at low current density.

4. Conclusions

In this study, Blue-TNA anode was first prepared by electrochemical reduction in formic acid. After electrochemical reduction, more Ti³⁺ (82%) was existed in Blue-TNA which was confirmed by the characterization of XPS, Raman, Mott-Schottky and CV. Compared with BDD anode, Blue-TNA had a better hydroxyl radical production activity (1.7×10^{-14} M) and TOC, COD removal, with a lower energy consumption of 9.9 kW h/(kg COD). Low pH, high current density and low Na₂SO₄ concentration favored for the contribution of ·OH while inhibited the formation of SO₄²⁻. Blue-TNA anode have a service life of 106 h at 2.5 mA/cm² in 0.1 M Na₂SO₄. The fresh anode could have a 5 cycles degradation of phenol, and after regeneration the electrode also had 4 cycles degradation. Blue-TNA anode also have an excellent performance of different contaminants of MB, 2,4-D, SMT, TC, RhB and *p*NP compared with other anodes. Therefore, Blue-TNA anode was promising and cost-effective for organic wastewater treatment. Due to the fact that Blue-TNA had an excellent performance at low current density, efforts could be made to further increase service life.

Declarations of interest

None.

Acknowledgments

This work was supported by Natural Science Foundation of China (nos. 21773129, 21811530274 and 21273120), Key Project of Natural Science Foundation of Tianjin (no. 16JCZDJC39300), National Key Research and Development Program (2016YFC0400706), National Special S&T Project on Water Pollution Control and Management (2017ZX07107002), 111 program, Ministry of Education, China (T2017002) and Fundamental Research Funds for the Central Universities.

Appendix A. Supplementary data

Supplementary material related to this article can be found, in the online version, at doi:<https://doi.org/10.1016/j.apcatb.2019.117902>.

References

- [1] I. Sires, E. Brillas, M.A. Oturan, M.A. Rodrigo, M. Panizza, Environ. Sci. Pollut. R. 21 (2014) 8336–8367.
- [2] G.H. Chen, Sep. Purif. Technol. 38 (2004) 11–41.
- [3] C.A. Martinez-Huitle, S. Ferro, Chem. Soc. Rev. 35 (2006) 1324–1340.
- [4] F.C. Moreira, R.A.R. Boaventura, E. Brillas, V.J.P. Vilar, Appl. Catal. B: Environ. 202 (2017) 217–261.
- [5] D.R. James, J. Wojciech, J.B. Nigel, Environ. Sci. Technol. 33 (1999) 1453–1457.
- [6] C. Raffaello, M.P. Anna, C.L. Maria, M. Michele, P. Simonetta, R. Fabrizio, Environ. Sci. Technol. 32 (1998) 3570–3573.
- [7] B. Boye, M.M. Dieng, E. Brillas, Environ. Sci. Technol. 36 (2002) 3030–3035.
- [8] Z.C. Wu, M.H. Zhou, Environ. Sci. Technol. 35 (2001) 2698–2703.
- [9] P. Canizares, J. Lobato, R. Paz, M.A. Rodrigo, C. Saez, Water Res. 39 (2005) 2687–2703.
- [10] J.X. Gao, G.H. Zhao, W. Shi, D.M. Li, Chemosphere 75 (2009) 519–525.
- [11] H. Lin, J. Niu, J. Xu, Y. Li, Y. Pan, Electrochim. Acta 97 (2013) 167–174.
- [12] M. Panizza, G. Cerisola, Chem. Rev. 109 (2009) 6541–6569.
- [13] F.C. Walsh, R.G.A. Wills, Electrochim. Acta 55 (2010) 6342–6351.
- [14] Z.X. Hu, M.H. Zhou, L. Zhou, Y.L. Li, C. Zhang, Environ. Sci. Pollut. R. 21 (2014) 8476–8484.
- [15] Y. Hou, X. Li, Q. Zhao, G. Chen, C.L. Raston, Environ. Sci. Technol. 46 (2012) 4042–4050.
- [16] Q. Wang, T. Jin, Z.X. Hu, L. Zhou, M.H. Zhou, Sep. Purif. Technol. 102 (2013) 180–186.
- [17] S. Nayak, B.P. Chaplin, Electrochim. Acta 263 (2018) 299–310.
- [18] C. Trellu, B.P. Chaplin, C. Coetsier, R. Esmilaire, S. Cerneaux, C. Causserand, M. Cretin, Chemosphere 208 (2018) 159–175.
- [19] S.O. Ganiyu, N. Oturan, S. Raffy, M. Cretin, R. Esmilaire, E. van Hullebusch, G. Esposito, M.A. Oturan, Water Res. 106 (2016) 171–182.
- [20] N. Oturan, S.O. Ganiyu, S. Raffy, M.A. Oturan, Appl. Catal. B: Environ. 217 (2017) 214–223.
- [21] S.O. Ganiyu, N. Oturan, S. Raffy, M. Cretin, C. Causserand, M.A. Oturan, Sep. Purif. Technol. 208 (2019) 142–152.
- [22] P. Geng, J. Su, C. Miles, C. Cominellis, G.H. Chen, Electrochim. Acta 153 (2015) 316–324.
- [23] A.M. Zaky, B.P. Chaplin, Environ. Sci. Technol. 47 (2013) 6554–6563.
- [24] A.M. Zaky, B.P. Chaplin, Environ. Sci. Technol. 48 (2014) 5857–5867.
- [25] H. Tokudome, M. Miyauchi, Angew. Chemie Int. Ed. English 44 (2005) 1974–1977.
- [26] X. Zhang, W. Hu, K. Zhang, J. Wang, B. Sun, H. Li, P. Qiao, L. Wang, W. Zhou, ACS Sustain. Chem. Eng. 5 (2017) 6894–6901.
- [27] H. Zhou, Y. Zhang, J. Phys. Chem. C 118 (2014) 5626–5636.
- [28] Y. Yang, M.R. Hoffmann, Environ. Sci. Technol. 50 (2016) 11888–11894.
- [29] M.S. Koo, K. Cho, J. Yoon, W. Choi, Environ. Sci. Technol. 51 (2017) 6590–6598.
- [30] J. Lee, W.Y. Choi, J. Yoon, Environ. Sci. Technol. 39 (2005) 6800–6807.
- [31] X. Chang, S.S. Thind, A.C. Chen, ACS Catal. 4 (2014) 2616–2622.
- [32] X. Cheng, Q. Cheng, X. Deng, P. Wang, H. Liu, Chemosphere 144 (2016) 888–894.
- [33] J. Jeong, C. Kim, J. Yoon, Water Res. 43 (2009) 895–901.
- [34] C. Kim, S. Kim, J. Lee, J. Kim, J. Yoon, ACS Appl. Mater. Inter. 7 (2015) 7486–7491.
- [35] J.Y. Kim, C. Kim, S. Kim, J. Yoon, J. Ind. Eng. Chem. 66 (2018) 478–483.
- [36] T.A. Kenova, G.V. Kornienko, O.A. Golubtsova, V.L. Kornienko, N.G. Maksimov, Environ. Sci. Pollut. R. 25 (2018) 30425–30440.
- [37] C. Han, Y. Ye, G. Wang, W. Hong, C. Feng, Chem. Eng. J. 347 (2018) 648–659.
- [38] G.D. Lee, J.L. Falconer, Catal. Lett. 70 (2000) 145–148.
- [39] W.D. Zhu, C.W. Wang, J.B. Chen, Y. Li, J. Wang, App. Surf. Sci. 301 (2014) 525–529.
- [40] G.G. Bessegato, F.F. Hudari, M.V.B. Zanoni, ElectrocJ.him. Acta 235 (2017) 527–533.
- [41] H.L. Gui, W. Zhao, C.Y. Yang, H. Yin, T.Q. Lin, Y.F. Shan, Y. Xie, H. Gu, F.Q. Huang, J. Mater. Chem. A 2 (2014) 8612–8616.
- [42] M.C. Liu, G.H. Zhao, K.J. Zhao, X.L. Tong, Y. Tang, Electrochim. Commun. 11 (2009) 1397–1400.
- [43] A. Zhang, F. Gong, Y. Xiao, X. Guo, F. Li, L. Wang, Y. Zhang, L. Zhang, J. Electrochim. Soc. 164 (2017) H91–H96.
- [44] W.J. Liao, J.W. Yang, H. Zhou, M. Muruganathan, Y.R. Zhang, Electrochim. Acta 136 (2014) 310–317.
- [45] H. Wu, D. Li, X. Zhu, C. Yang, D. Liu, X. Chen, Y. Song, L. Lu, Electrochim. Acta 116 (2014) 129–136.
- [46] N. Liu, V. Haublein, X. Zhou, U. Venkatesan, M. Hartmann, M. Mackovic, T. Nakajima, E. Speicker, A. Osvet, L. Frey, P. Schmuki, Nano Lett. 15 (2015) 6815–6820.
- [47] C. Kim, S. Kim, J. Choi, J. Lee, J.S. Kang, Y.E. Sung, J. Lee, W. Choi, J. Yoon, Electrochim. Acta 141 (2014) 113–119.
- [48] C. Kim, S. Lee, S. Kim, J. Yoon, Electrochim. Acta 222 (2016) 1578–1584.
- [49] X.M. Yu, M.H. Zhou, Y.S. Hu, K.G. Serrano, F.K. Yu, Environ. Sci. Pollut. R. 21 (2014) 8417–8431.
- [50] J.J. Cai, M.H. Zhou, W.L. Yang, Y.W. Pan, X.Y. Lu, K.G. Serrano, Chemosphere 212 (2018) 784–793.
- [51] J.H. Kou, Z.S. Li, Y.P. Yuan, H.T. Zhang, Y. Wang, Z.G. Zou, Environ. Sci. Technol. 49 (2009) 2919–2924.
- [52] J. Radjenovic, M. Petrovic, J. Hazard. Mater. 333 (2017) 242–249.
- [53] S.H. Yuan, P. Liao, A.N. Alshawabkeh, Environ. Sci. Technol. 48 (2014) 656–663.
- [54] D. Bejan, E. Guinea, N.J. Bunce, Electrochim. Acta 69 (2012) 275–281.
- [55] C.J. Liang, Z.S. Wang, C.J. Bruehl, Chemosphere 66 (2007) 106–113.
- [56] L.C. Chen, C.J. Lei, Z.J. Li, B. Yang, X.W. Zhang, L.C. Lei, Chemosphere 210 (2018) 516–523.
- [57] H. Zhang, Z. Wang, C.C. Liu, Y.Z. Guo, N. Shan, C.X. Meng, L.Y. Sun, Chem. Eng. J. 250 (2014) 76–82.
- [58] Y. Yang, L.C. Kao, Y.Y. Liu, K. Sun, H.T. Yu, J.H. Guo, S.Y.H. Liou, M.R. Hoffmann, ACS Catal. 8 (2018) 4278–4287.
- [59] L. Gan, Y.F. Wu, H.O. Song, C. Lu, S.P. Zhang, A.M. Li, Chemosphere 226 (2019) 329–339.
- [60] G.H. Zhao, J.X. Gao, S.H. Shen, M.C. Liu, D.G. Li, M.F. Wu, Y.Z. Lei, J. Hazard. Mater. 172 (2009) 1076–1081.
- [61] R. Berenguer, J.M. Sieben, C. Quijada, E. Morallón, Appl. Catal. B: Environ. 199 (2016) 394–404.
- [62] J.T. Xing, D.H. Chen, W. Zhao, X.L. Peng, Z.L. Bai, W.W. Zhang, X.X. Zhao, RSC Adv. 5 (2015) 53504–53513.
- [63] E. Brillas, B. Boye, I. Sires, J.A. Garrido, R.M. Rodriguez, C. Arias, P.L. Cabot, C. Cominellis, Electrochim. Acta 49 (2004) 4487–4496.
- [64] A. El-Ghenemy, P.L. Cabot, F. Centellas, J.A. Garrido, R.M. Rodriguez, C. Arias, E. Brillas, Electrochim. Acta 90 (2013) 254–264.
- [65] P. Jiang, J.T. Zhou, A.L. Zhang, Y.J. Zhong, J. Environ. Sci. China (China) 22 (2010) 500–506.
- [66] D. Maharanan, J.F. Niu, D. Gao, Z.S. Xu, J.H. Shi, Water Environ. Res. 87 (2016) 304–311.
- [67] G.R. de Oliveira, N.S. Fernandes, J.V. de Melo, D.R. da Silva, C. Urgeghe, C.A. Martinez-Huitle, Chem. Eng. J. 168 (2011) 208–214.